Cometary Materials Originating from Interstellar Ices: Clues from Laboratory Experiments

A. Fresneau, N. Abou Mrad, L. L. S. d'Hendecourt, F. Duvernay, L. Flandinet, F. -R. Orthous-Daunay, V. Vuitton, R. Thissen, T. Chiavassa, G. Danger

The Astrophysical Journal, 837:168 (8pp), 2017 March 10 https://doi.org/10.3847/1538-4357/aa618a

Cometary Materials Originating from Interstellar Ices: Clues from Laboratory Experiments

A. Fresneau[1], N. Abou Mrad[1], L. LS d'Hendecourt[1,2,3], F. Duvernay[1], L. Flandinet[4], F.-R. Orthous-Daunay[4], V. Vuitton[4], R. Thissen[4], T. Chiavassa[1], and G. Danger[1]
[1] Aix-Marseille Université, PIIM UMR-CNRS 7345, F-13397 Marseille, France; gregoire.danger@univ-amu.fr
[2] Univ. Paris-Sud, Université de Paris-Saclay, Astrochimie et Origines, Institut d'Astrophysique Spatiale, UMR 8617, Orsay F-91405, France
[3] CNRS, Orsay F-91405, France
[4] Université Grenoble Alpes, CNRS, IPAG, Grenoble F-38000, France
Received 2016 December 21; revised 2017 February 15; accepted 2017 February 16; published 2017 March 15

Abstract

We use laboratory experiments to derive information on the chemistry occurring during the evolution of astrophysical ices from dense molecular clouds to interplanetary objects. Through a new strategy that consists of coupling very high resolution mass spectrometry and infrared spectroscopy (FT-IR), we investigate the molecular content of the organic residues synthesized from different initial ice compositions. We also obtain information on the evolution of the soluble part of the residues after their over-irradiation. The results give insight into the role of water ice as a trapping and diluting agent during the chemical evolution. They also give information about the importance of the amount of ammonia in such ices, particularly regarding its competition with the carbon chemistry. All of these results allow us to build a first mapping of the evolution of soluble organic matter based on its chemical and physical history. Furthermore, our results suggest that interstellar ices should lead to organic materials enriched in heteroatoms that present similarities with cometary materials but strongly differ from meteoritic organic material, especially in their C/N ratios.

Key words: astrochemistry – comets: general – techniques: spectroscopic – methods: laboratory: molecular – molecular processes – solid state: refractory

1. Introduction

The study of the organic matter found in extraterrestrial bodies such as comets and asteroids, as well as meteorites found on Earth, is an ongoing quest that started in the second half of the 20th century (Hayes 1967) and makes constant progress related to sampling performance, such as micrometric sample handling, sensitivity, and resolution. Mass spectrometry in situ analysis of cometary comae has revealed the presence of several organic molecules (Bockelée-Morvan et al. 2004), and glycine—the smallest of the amino acids—has been detected on comets 81P/Wild 2 (Elsila et al. 2009) and 67P/Churyumov–Gerasimenko (Altwegg et al. 2016) by the *Stardust* and *Rosetta* missions, respectively. By contrast, the soluble organic matter (SOM) from primitive meteorites has revealed hydroxy acids (Pizzarello et al. 2010), amino acids (Cronin & Moore 1971; Burton et al. 2014; Callahan et al. 2014), sugar derivatives (Cooper et al. 2001; Cooper & Rios 2016), and hydrocarbons (Martins et al. 2015). Untargeted analyses with very high resolution mass spectrometry (VHRMS) show that the SOM contains tens of thousands of different molecules (Schmitt-Kopplin et al. 2010).

Our work focuses on producing analogs of interstellar or pre-cometary ice and studying their chemical evolution throughout their exposure to energetic processes, such as those anticipated during the different steps of the formation of a solar system. We simulate this evolution in the laboratory (Greenberg et al. 1995). In this context, ices made of mixtures of H_2O, NH_3, and CH_3OH are first irradiated with VUV photons at Lyα (121 nm) and then heated to room temperature (295 K), leading to the production of a refractory organic residue (Briggs et al. 1992). Targeted gas chromatography coupled with mass spectrometry (GC-MS) analyses of this residue show the presence of amino acids (Nuevo et al. 2007) and sugars (de Marcellus et al. 2015; Meinert et al. 2016), for example. Untargeted analyses using VHRMS reveal that the residue contains thousands of molecules with molecular masses up to 4000 Da (Danger et al. 2013, 2016). Such diversity reminds us of the complex content of the SOM of meteorites (Schmitt-Kopplin et al. 2010; Somogyi et al. 2016) and suggests that residues formed in the laboratory from the energetic processing of interstellar/pre-cometary ice analogs can serve as interesting templates for studying the chemical evolution of organic matter in astrophysical environments.

The goal of this work is to present a new analytical strategy to get a better understanding of the chemistry at the origin of these organic residues. Through a global analysis of the residues using VHRMS and Fourier transform infrared spectroscopy (FT-IR), we investigate the impact of variations in the residue formation process (composition of the initial ice, effect of over-irradiation). These investigations provide an adequate representation of the data that gives insight into the condensed phase chemistry and could eventually allow prediction of the initial ice composition from which real extraterrestrial soluble organic material evolved.

2. Experimental Details

2.1. Residue Syntheses

The first step consists of producing samples that are considered analogous to the organic residues originating from the processing of icy mantles of interstellar grains. The experimental setup has been described in detail in previous work (Nuevo et al. 2007). Succinctly, a gas mixture containing H_2O, CH_3OH, and NH_3 is prepared in a stainless steel line pumped down to 10^{-6} mbar beforehand. The H_2O was purified

Table 1
Parameters Used for Each of the 15 Samples

H_2O:CH_3OH:NH_3 Ratio	Deposition/Irradiation (hr)	Over-Irradiation of the Residue	Number of Replicates
3:1:1	48	⋯	3
3:1:0.2	48	⋯	3
3:1:5	48	⋯	2
10:1:1	48	⋯	3
3:1:1	48	48 hr	3
3:1:1	16	⋯	1

with a Millipore Direct Q5 system, the CH_3OH (99.9%) was purchased from Aldrich, and the NH_3 (99.98%) was purchased from Messer. The mixture is then deposited on an MgF_2 window cooled down to 77 K inside a vacuum chamber (10^{-7} mbar). The gas condenses, and an ice forms on the window. During the ice buildup, an H_2 discharge lamp is used to irradiate the ice with VUV photons (mainly Lyα). After 48 hr of combined deposition and irradiation, the window is slowly warmed up to 295 K (~0.1 K minute^{-1}). The composition of the sample is monitored in situ with an FT-IR spectrometer attached to the vacuum chamber. The IR spectra (4000–1000 cm^{-1}, 500 scans, 2 cm^{-1} resolution) allow control of the deposition rate and the composition of the ice, and they give us insight into the composition of the residue that remains on the surface of the window at room temperature. At this stage, some of the residues are VUV irradiated for an extra 48 hr at 295 K (without gas deposition). This is called "over-irradiation." The residues are then retrieved from the vacuum chamber and placed inside stainless steel sample holders sealed under 1 atm of argon to avoid contamination until analysis. Fifteen samples were produced following the protocol. A list of the various parameters used for each sample is given in Table 1.

Although most features will be shared by all samples, the relative intensities of those features can vary between samples, depending on the composition of the initial ice (Table 1). To compare the spectra, we define a parameter α that allows us to follow the ratio between the IR bands located at 1745 cm^{-1} (acid or ester groups) and 1665 cm^{-1} (carbonyls containing nitrogen functions). Since we modify the fraction of nitrogen and oxygen in the initial ice, this parameter will allow a correlation with the amount of heteroatoms in residues:

$$\alpha = \frac{A_{1745\ \mathrm{cm^{-1}}}}{A_{1665\ \mathrm{cm^{-1}}}},$$

where $A_{1745\ \mathrm{cm^{-1}}}$ is the area of the ν_{CO} band of (nitrogen-free) ester or acid (f) at 1745 cm^{-1} and $A_{1665\ \mathrm{cm^{-1}}}$ is the area of the ν_{CO} band of (nitrogen-containing) amide or carbamic acid (g) at 1665 cm^{-1}. The value of $\widetilde{\alpha}$ is the mean of the α ratios of the different residues formed from identical ices. The values of $\widetilde{\alpha}$ are summarized in Table 3. The lower the value of $\widetilde{\alpha}$, the higher the nitrogen content of the residue.

2.2. Residue VHRMS Analyses

In order to be analyzed with the FT-Orbitrap (LTQ Orbitrap XL), each residue is solubilized in ultrapure methanol. This is performed by rinsing the window with 5 × 50 μl of methanol with a micropipette. All residues that have not been over-irradiated are totally soluble in methanol. No residue remains on the MgF_2 window after rinsing (at the FT-IR detection limit). By contrast, the residues that have been over-irradiated for 48 hr leave a thin layer of dark insoluble matter that cannot be removed even after soaking the window for several hours in methanol, toluene, or water (de Marcellus et al. 2017). For these residues, only the soluble fraction retrieved from the micropipette rinsing is analyzed with the FT-Orbitrap. Since some methanol evaporation has occurred during the residue recovery, we added methanol in the Eppendorf tube up to 200 μl for each sample. Fifty μl of this solution were then collected and diluted with 1950 μl of methanol. This last solution was injected with a Hamilton gastight syringe at a rate of 3 μl minute^{-1} inside the electrospray ionization (ESI) source of the FT-Orbitrap. The following conditions were used to acquire the mass spectra: needle voltage, 3.7 kV; heated capillary temperature, 275° C; and tube lens voltage, −131 V and +90 V for the negative and positive ESI modes, respectively. The resolution was set to 100,000 at m/z 400. A detailed description of the LTQ Orbitrap XL instrument used can be found in Danger et al. (2013). Data is acquired from the spectral window (selected ion monitoring) m/z 200–400. A blank is recorded before each sample run under the same conditions. The blank consists of ultrapure methanol that has been pipetted in an Eppendorf tube.

Table 2
Position and Attribution of the IR Bands of the Residues

Label in Figure 1	Wavenumber (cm^{-1})	Vibration Mode
a	3245	ν_{OH}
b	3203	ν_{NH}
c	2930	ν_{CH} as
d	2874	ν_{CH} s
e	2148	$\nu_{N=C=O}$
f	1745	$\nu_{C=O}$ of esters/acids (Muñoz Caro & Schutte 2003)
g	1665	$\nu_{C=O}$ of amides/carbamic acid (Muñoz Caro & Schutte 2003)
h	1638	δ_{NH} or $\nu_{C=N}$
i	1595	ν_{asCOO^-} (Schutte et al. 1999)
j	1460	δ_{CH} (CH_3)
k	1372	δ_{CH2} of HMT (Bernstein et al. 1995)
l	1343	ν_{sCOO^-}
m	1299	no attribution
n	1233	ν_{CN} of HMT (Bernstein et al. 1995)
o	1005	ν_{CN} of HMT (Bernstein et al. 1995)

Note. Vibration mode: stretching (ν), bending (δ). Type of vibration mode: asymmetric (as), symmetric (s).

3. Results

General considerations. The IR spectra of the residues at 295 K are displayed in Figure 1. For the sake of clarity, only one spectrum for each ice composition is shown. The IR spectra of all the residues, including the replicates, can be found in the Appendix. All IR bands in the range 4000–1000 cm^{-1} (resolution 2 cm^{-1}) are marked with letters in Figure 1, and their attributions are reported in Table 2. Most of the IR features are visible in all of the samples, indicating that they mainly include the same functional groups. In particular, hexamethylenetetramine (HMT) is detected in all spectra, identified by two characteristic C–N stretching bands

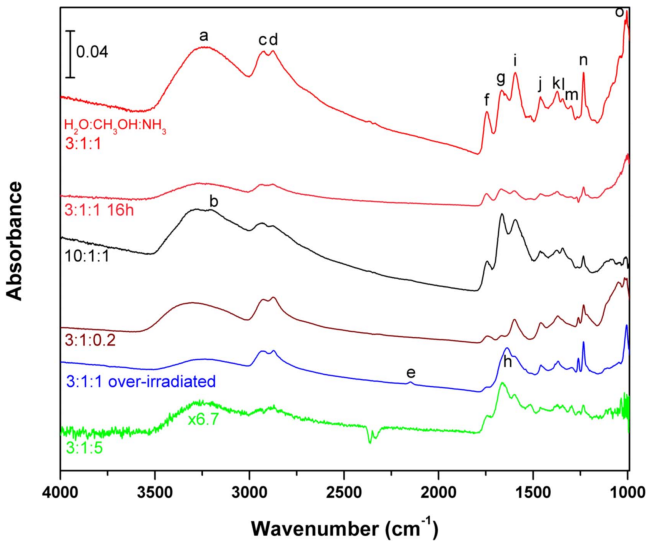

Figure 1. IR spectra of one of each triplicate residue presented in Table 1, at 295 K. The 3:1:5 residue spectrum has been magnified 6.7 times for clarity. The IR bands are marked with letters and reported in Table 2.

(ν_{CN}) at 1233 and 1005 cm^{-1} (Vinogradoff et al. 2011). It is known that VUV irradiation followed by the warming of the H_2O:CH_3OH:NH_3 ices readily produces HMT (Bernstein et al. 1995; Vinogradoff et al. 2011, 2012). The IR spectroscopy analyses give a global view of the chemical molecular functions present in the residues. Nevertheless, the molecular diversity is expected to be much more important than that observed by the IR analyses, since the most intense IR features mask this molecular diversity (Danger et al. 2013). We therefore complete the FT-IR analysis with a VHRMS analysis to analyze the soluble part of the same residues in order to determine whether the behavior observed with IR spectroscopy is also observed when taking into account the whole molecular diversity. Table 3 summarizes the processed data from VHRMS analyses of the various residues in the range m/z 200–400. The average and standard deviations of the double bond equivalent (DBE) and the N/C and O/C ratios are reported for each triplicate of residues in Figure 2.

The IR spectra of each residue triplicate show very good reproducibility for each of the different ice compositions (Figure 4). This is particularly remarkable because some samples were made years apart by different operators. This is confirmed by the VHRMS analyses, which show that variations of the ratios between the different residues are significant enough compared to the standard deviations of one residue triplicate that we can assess that those variations are due to the different ice mixtures used to prepare the residues or to residue over-irradiation (Figure 2). Compared to the FT-IR analyses, VHRMS shows that two distinct distributions are detected in each sample (Figure 2). The first, which we call the carbon distribution, is detected in both positive and negative ionization modes (Figure 5) and shows average N/C ratios between 0.2 and 0.6, as well as an average DBE in the 5–6 range. The second, which we call the nitrogen-enriched distribution, is detected only in the positive ionization mode (Figure 5) and has noticeably higher average N/C ratios (between 0.9 and 1.6) and DBE (between 7 and 9). Molecules with such DBE and N/C could be triazine-like structures (Gautier et al. 2016). Other molecules can present characteristics such as HCN polymers, but they should also be detected in the negative ionization mode (Somogyi et al. 2012; Bonnet et al. 2013).

Effect of the duration of sample formation. The effect of the duration of the deposition and simultaneous irradiation on the composition of the residue can be evaluated by comparing the residues obtained from the 3:1:1 ices (H_2O:CH_3OH:NH_3) deposited and irradiated for either 48 hr or 16 hr. The same features are observed in both IR spectra, with an overall smaller absorbance for the 16 hr residue. Similar to the IR analyses, the VHRMS analysis shows that deposition time has very little or no effect on the residue composition. Indeed, the O/C and N/C ratios, as well as the DBE, of the 16 hr residue fall within the standard deviation of the values found for the 48 hr residues for both regular and nitrogen-enriched distributions. The duration of the simultaneous deposition and irradiation simply affects the amount of the final residue and does not significantly impact the residue composition itself.

Effect of NH_3 in residue composition. If we compare the IR spectra of the residues originating from the ices containing 3:1:0.2, 3:1:1, and 3:1:5 ratios (H_2O:CH_3OH:NH_3), we notice that ã decreases from 5 to 0.4 (Table 3) accordingly with the increase of NH_3 in the initial ice. It shows that the more NH_3 in the initial ice, the more nitrogen is incorporated into the residue, which is an intuitive result. These results confirm observations made by Bernstein et al. in which residues formed from H_2O:CH_3OH:CO:NH_3 in 10:5:1:1 or 10:5:1:4.5 ratios present an increase of bands characteristic of amide or nitrogen functions when the fraction of NH_3 increases in the initial ice (Bernstein et al. 1995).

VHRMS analyses confirm this observation, since the N/C ratio increases in the residue with the initial fraction of NH_3 in the ice (Figure 2 and Table 3). This is observed for both distributions and is even more pronounced in the nitrogen-enriched distribution. There is thus a direct link between the fraction of NH_3 in the initial ice and the fraction of nitrogen in the residue. By contrast, the O/C ratio does not vary significantly. The H_2O:CH_3OH ratios (3:1) are the same in the initial ices, implying that the fraction of carbon and oxygen available to react in the ice is identical. The average number of O atoms is rather stable between residues (Table 3), while the number of nitrogen atoms increases from 3.6 to 6.0 when passing from 3:1:0.2 to 3:1:5. Furthermore, a nonnegligible decrease in the number of carbon atoms is also observed (from 12.4 to 10.3). This most certainly is the signature of a competition in the formation of the carbon skeleton of molecules and implies a decrease of the amount of C in the residue.

Effect of H_2O in residue composition. The comparison of the residues coming from the 10:1:1, 3:1:1, and 3:1:5 (H_2O:CH_3OH:NH_3) ice mixtures also provides information on the role played by water in the residue formation. Apart from the difference in total absorbance, the IR spectrum of the 3:1:5 residue shows an interesting resemblance to that of the 10:1:1 residue. The value of $\tilde{\alpha} = 0.3$ for the 10:1:1 residue is close to the value of $\tilde{\alpha} = 0.4$ for the 3:1:5 residue, meaning that it is enriched in nitrogen.

VHRMS analyses confirm these first IR analyses. Interestingly, for both the carbon and nitrogen distributions, the N/C ratio of the 10:1:1 residues is higher than that of the 3:1:1 residues, even though there is a lower fraction of nitrogen available in the 10:1:1 ice (1/12) than in the 3:1:1 ice (1/5). Furthermore, the nitrogen incorporation is extremely effective,

Table 3
Average Number of Elements per Attribution, Elemental N/C and O/C Ratios, and DBE for Each Type of Residue and Ice Described in Table 1

H_2O:CH_3OH:NH_3	C_x	H_y	N_z	O_w	N/C	O/C	DBE	$\widetilde{\alpha}$
Initial Ice								
3:1:0.2	1	5.6	0.2	4	0.2	4	0	⋯
3:1:1	1	9	1	4	1	4	0	⋯
3:1:5	1	25	5	4	5	4	0	⋯
10:1:1	1	27	1	11	1	11	0	⋯
Carbon Distribution								
3:1:0.2	12.4	19.1	3.6	3.9	0.29	0.32	5.69	5
3:1:1	11.7	18.1	4.0	4.1	0.34	0.35	5.72	0.9
3:1:5	10.3	18.8	6.0	3.1	0.59	0.31	4.91	0.4
10:1:1	11.1	18.6	5.6	2.9	0.5	0.27	5.53	0.3
3:1:1 over-irradiated	12.5	19.7	4.8	2.4	0.38	0.19	6.04	⋯
3:1:1 16 hr	11.9	18.9	4.6	3.3	0.38	0.28	5.74	0.9
Nitrogen-Enriched Distribution								
3:1:0.2	8.7	12.3	8.3	3.0	0.96	0.35	7.64	⋯
3:1:1	8.1	11.4	9.4	2.2	1.17	0.27	8.05	⋯
3:1:5	7.3	12.4	11.5	1.3	1.57	0.18	7.86	⋯
10:1:1	7.2	11.4	10.8	1.6	1.51	0.22	7.92	⋯
3:1:1 over-irradiated	7.6	11.9	9.8	1.5	1.28	0.20	7.55	⋯
3:1:1 16 hr	7.7	11.2	9.9	1.8	1.29	0.24	8.04	⋯

Note. For instance, for the residue 3:1:0.2, $x = 12.4$, $y = 19.1$, $z = 3.6$, and $w = 3.9$, referring to the general formula $C_xH_yN_zO_w$. The definition of $\widetilde{\alpha}$ is given in Section 2.1. Details of the residue formation are displayed in Section 2.2.

since the amount of nitrogen incorporated into a 10:1:1 residue is equivalent to that obtained for a 3:1:5 residue, which originates from an ice containing 5 times more nitrogen (Table 3). Moreover, the number of O atoms in the 10:1:1 residues is also very similar to that in the 3:1:5 residues, again for both distributions. This nitrogen enrichment is also observable in the 3:1:0.2 residue. In the initial ice, the N/C ratio is 0.2 (Table 3), while in the residue it is 0.29, the O/C ratio decreasing by one order. The nitrogen enrichment in the residue is also visible in XANES analyses of the residues formed from the ices containing H_2O:CH_3OH:CO:NH_3 in a 100:50:1:1 ratio (Nuevo et al. 2011). The N/C ratio exhibits a nitrogen enrichment of 14, while the O/C fraction is divided by 6, from the original ice to residue abundance. This is counterintuitive, as we would expect a lower amount of nitrogen in the 10:1:1 residue due to NH_3 being more diluted than in a 3:1:1 ice and a higher amount of oxygen due to its higher abundance in the initial ice. This confirms the results previously observed by Henderson et al. on the reactivity of water ice mixtures (Henderson & Gudipati 2015). These observations suggest that an increase of water or ammonia in the initial ice leads to the same effect: a higher incorporation of nitrogen in the residue.

An explanation for this nitrogen enrichment could come from the excess of H_2O. It has been shown that water can trap reactants such as NH_3 in the ice and allow them to react above their desorption temperature, permitting reactions otherwise impossible in the solid phase (Fresneau et al. 2014). This phenomenon could increase the proportion of nitrogen incorporated into the residue from NH_3 (Theule et al. 2013), which would explain the low value of $\widetilde{\alpha}$. H_2O could also impact the radical reactivity by spacing the various radicals, such as NH_2 that limit their local recombination into NH_3 due to the fast diffusion and desorption at this temperature of H. The NH_2 radicals are maintained free for a more diverse reactivity with radicals produced from methanol in bulk during the ice warming (Öberg et al. 2010; Butscher et al. 2016; Öberg 2016). This provides a richer chemistry, especially for nitrogen radical chemistry, as shown by the increase of nitrogen in the residue. This phenomenon could explain the increase in the residue abundance observed in the IR spectra by Muñoz Caro et al. when passing from an ice containing H_2O:CH_3OH:NH_3 in a 2:1:1 ratio to a 20:1:1 ratio (Muñoz Caro & Schutte 2003).

Impact of residue over-irradiation on the soluble organic material. Finally, the 3:1:1 over-irradiated residue was compared to a regular 3:1:1 residue. As described by de Marcellus et al. (2017), once the residue is over-irradiated, an insoluble material is formed on the top of the residue. The remaining soluble fraction is then recovered in methanol, and the insoluble part is thus not analyzed with VHRMS. The VHRMS analysis shows a decrease of the O/C ratio from 0.35 to 0.19 after over-irradiation, while the N/C ratio does not significantly change. A possible explanation for the decrease of the O/C ratio could be the decarboxylation or dehydration of some carbonyl groups, which would release CO_2 and/or H_2O in the gas phase, finally depleting O in the residue. The degradation of the carbonyl groups is supported by the decrease of the band at 1745 cm^{-1} relative to the other bands. This band corresponds to acids or esters that formed CO, CO_2, and H_2O under the VUV irradiations (Lundell & Räsänen 1997; Maçôas et al. 2004). At 295 K, CO, CO_2, and H_2O are probably directly released in the gas phase, depleting the O content of the residue as observed with VHRMS. Furthermore, the isocyanate (R–N=C=O) band observed at 2148 cm^{-1} after over-irradiation could result from the degradation of amide (Duvernay et al. 2005), or possibly carbamic acid functions (Bossa et al. 2008) under over-irradiation. The band observed at 1638 cm^{-1} could also be assigned to amine coming from the

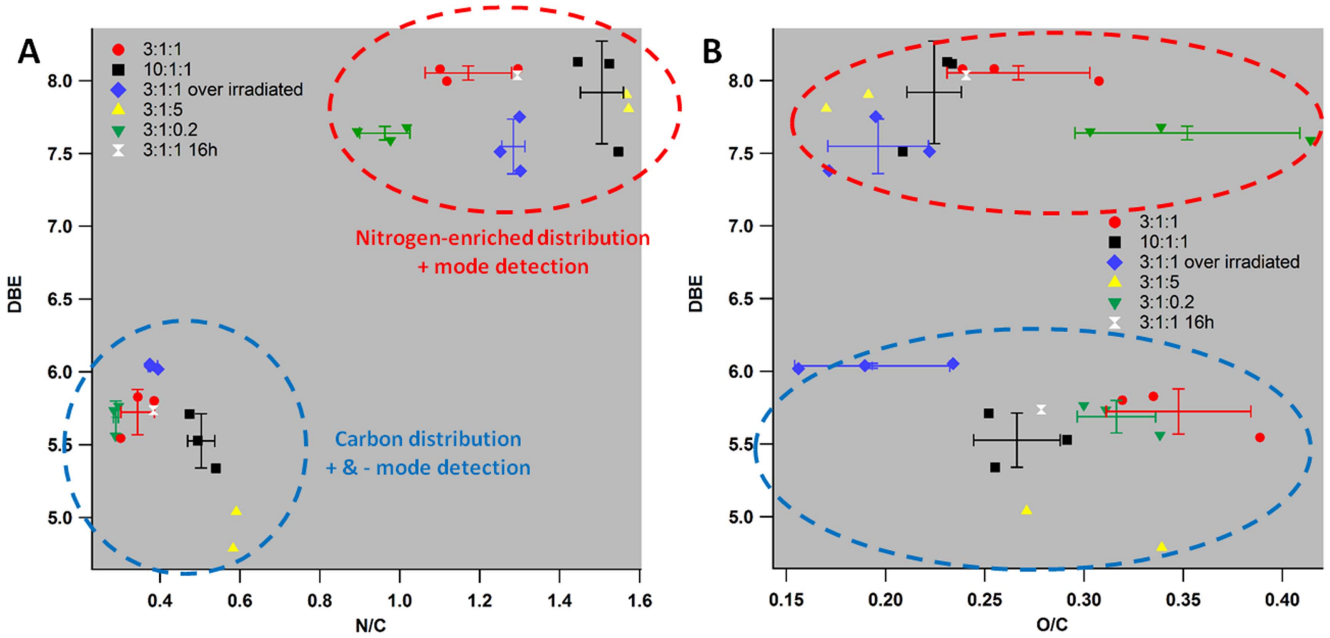

Figure 2. Diagrams representing the means and standard deviations of the DBE and the N/C and O/C ratios of the residues presented in Table 3. Each point corresponds to the average of all attributions found in the m/z range 200–400 (Figure 5). Standard deviations are obtained from the triplicates. In panel (a), the blue ellipsis delimits the carbon distribution that is detected in the positive and negative ionization modes, while the red ellipsis delimits the nitrogen-enriched distribution that is detected in the positive mode only.

amide degradation (Duvernay et al. 2005). These IR observations demonstrate that chemical functions bearing a carbonyl group, such as amide or acid, are degraded by the over-irradiation and lead to oxygen depletion detectable from VHRMS analyses.

Finally, the VHRMS analysis also shows that the over-irradiation of the initial organic residue at room temperature affects the soluble fraction, since the insoluble material is formed due to over-irradiation of the soluble part.

4. Astrochemical Discussion

If we look to the ice composition of low-mass young stellar objects that can represent the first step of the solar system's evolution, on average, their ices are formed of H_2O:CO:CO_2:CH_3OH:NH_3 in a ratio of 100:44:31:13:6 (Boogert et al. 2015). This composition is close to our 3:1:0.2 analog. We do not have CO and CO_2 in our analogs, but experiments with the carbon oxides give similar N and O enrichments in the residues (Muñoz Caro & Schutte 2003; Nuevo et al. 2011) of our analogs compared to the SOM of meteorites. In our experiments, CO and CO_2 are formed from the processing of CH_3OH, even if their presence in the initial ice can affect some branching ratios; the chemical composition of the final residue is slightly affected. One can also argue that only UV processing is used in these experiments, and that a higher energetic process may account for some variations in the N and O content of the residues. However, an IR comparison of the residues formed from VUV or ion irradiations has not shown particular differences in the residue compositions (Muñoz Caro et al. 2014). Our experiments are thus representative of the general interstellar ice processing during the formation of a planetary system.

Our measurements provide the first insight into the evolution of the residues based on their modes of formation and alteration

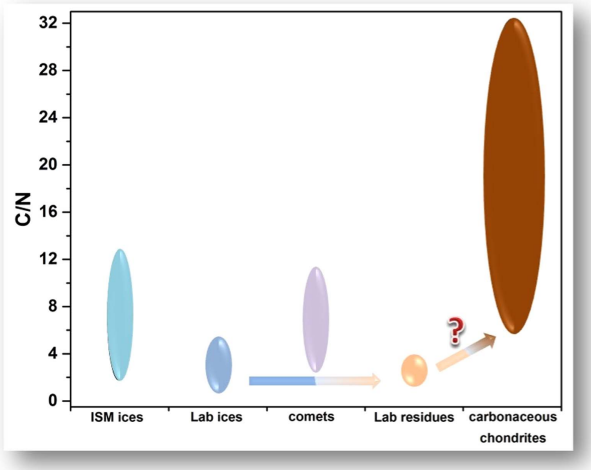

Figure 3. C/N ratios in various interstellar medium (ISM) ices, comets, and carbonaceous chondrites, as well as for the laboratory ices and residues. The values of the ISM ices, comets, and carbonaceous chondrites are taken from Bergin et al. 2015. The values of the laboratory ices and residues are taken from this work. Ovals refer to the C/N range observed for each object.

in order to get closer to the organic matter of interplanetary objects. Investigations of the C/N ratio of various astrophysical objects (Bergin et al. 2015) show that our ice analogs are representative of interstellar ices (ice analog C/N from 1 to 5 versus 2 to 12 for interstellar ices). Furthermore, the C/N ratio of comets is near that of our residue (residue produced from the 10:1:1 ice analog, C/N 2 versus 4 for comets). However, the C/N ratio strongly diverges from that of meteorites, which present much a higher C/N ratio than our residues (Figure 3). This is confirmed by the SOM FT-ICR analysis of the Murchison meteorite (Schmitt-Kopplin et al. 2010), which gives an average elemental composition of N/C = 0.03,

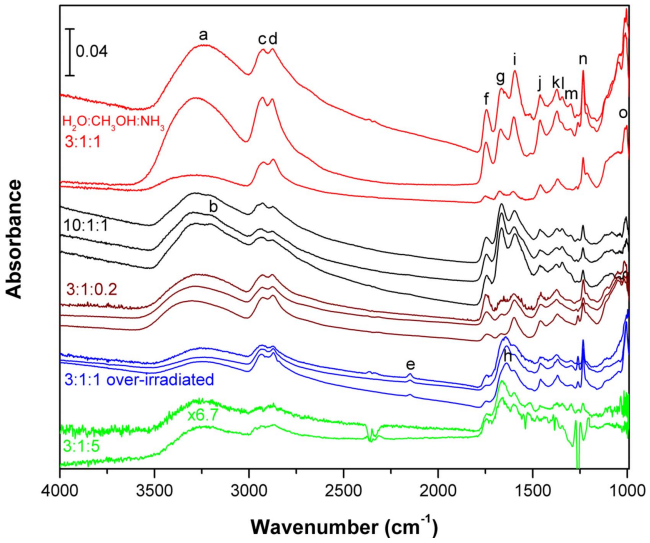

Figure 4. IR spectra of all of the residues described in Table 1, at 295 K. Separate experiments using the same ice ratios are displayed in the same color. The 3:1:5 residue spectra have been magnified 6.7 times for clarity. The IR bands are marked with letters and reported in Table 2. We can see the good reproducibility for each ice composition. Only the 3:1:1 residues show a significant variability in total absorbance. However, the band ratios are still preserved between the 3:1:1 residues.

O/C = 0.2, and H/C = 1.55, i.e., a much lower N/C than that of our residue. However, the precursors of SOM have undergone more evolution than our residue (Le Guillou & Brearley 2014; Le Guillou et al. 2014). Our residue represents only the organic material that comes from the astrophysically representative interstellar ice evolution under UV irradiation before its alteration inside asteroids.

Our results show for the first time that even if the molecules of the initial ice are diluted in H_2O, the organic residues are still enriched in nitrogen; this suggests that interstellar ices can lead to residues enriched in nitrogen, in contrast to the SOM of carbonaceous meteorites. This enriched material can then be incorporated with the primitive ices inside solar system minor bodies, such as comets and asteroids. In comets, this material originating from the processing of interstellar ices evolves only slightly, explaining the rather minor increase of the C/N ratio observed between interstellar ices and comets (Bergin et al. 2015). We have to pursue the diversification of the processes applied to the ice and residue. This will allow us to identify the determinant parameters that lead to material similar to the SOM and insoluble organic matter (IOM) of meteorites and that could explain the N and O impoverishments observed in the SOM compared to comet materials. Particularly, secondary processing inside the parent bodies of meteorites, such as hydrothermal alteration, has to be investigated to determine whether the evolution of our soluble organic material formed from astrophysically representative ices can be a source of the SOM observed in meteorites (Bergin et al. 2015). Experiments on the hydrothermal treatment of diverse IOM meteorites have indeed shown an important release of ammonia, which probably results from the degradation of chemical functions bearing nitrogen, such as amines (Pizzarello et al. 2011; Pizzarello & Williams 2012). Therefore, after the accretion of soluble and insoluble material formed on grains (de Marcellus et al. 2017), this alteration could induce an important loss of nitrogen inside the parent bodies of meteorites.

5. Conclusion

We have developed a methodology coupling in situ residue analysis by IR spectroscopy with ex situ high-resolution mass spectrometry. These two methods are complementary and give valuable information about the impact of the initial composition of the ices on the formation of the residues, as well as the effect of residue alteration. Beyond the changes in the molecular composition of the residues, these analyses give information on the reactivity occurring during their formation. Our analysis shows that water plays an important role in the chemistry leading to these residues. H_2O induces an increase in nitrogen incorporation within the residues. It creates a molecular trapping and probably impacts radical reactions by diluting radicals at low temperatures, which limits their direct recombination. This process leads to the formation of new C–N bonds. However, higher amounts of water in the initial ice do not increase the amount of oxygen present within the residues. This would imply that the oxygen present in the molecules constituting the residues mainly comes from methanol, not from H_2O, which confirms previous results observed (Henderson & Gudipati 2015). An increase of the amount of NH_3 within the ice leads to higher nitrogen incorporation into the residue, similar to an increase of the amount of H_2O. This can be explained by an enrichment of nitrogen molecules during the combination of nitrogen and carbon radicals at low temperatures and by the thermal reactions of NH_3 or amino derivatives on the carbonyl group of aldehydes or ketones. We also confirm that an excess of H_2O increases the abundance of the residue due to its trapping effect up to 180 K. We also show that residue alteration by over-irradiation, which leads to insoluble material, creates measurable changes in the soluble part of the residue, with a decrease of the oxygen amount. This indicates that over-irradiation also alters a part of the soluble material sufficiently to make a detectable difference compared to the initial soluble material. Finally, our results support the astrophysical scenario that links cometary materials with the evolution of interstellar icy grains during the whole process from the final molecular cloud stages to the solar nebula formation. The processing of interstellar ices would indeed form organic residues enriched with heteroatoms, such as nitrogen and oxygen, which differ from the heteroatom composition of carbonaceous chondrites.

This work has been funded by the French national programs "Physique Chimie du Milieu Interstellaire" (P.C.M.I, Institut National des Sciences de l'Univers, Centre National de la Recherche Scientifique), "Programme National de Planétologie" (P.N.P, INSU-CNRS), the Centre National d'Etudes Spatiales (CNES) from its exobiology program, and a PhD grant from the Région Provence Alpes Côte d'Azur (PACA). This work was further supported by the ANR projects RAHIIA_SSOM (Grant ANR-16-CE29-0015-01), VAHIIA (Grant ANR-12-JS08-0001), and PeptiSystems (Grant ANR-14-CE33-0020-02) of the French Agence Nationale de la Recherche, and, finally, the Fondation Aix-Marseille Université.

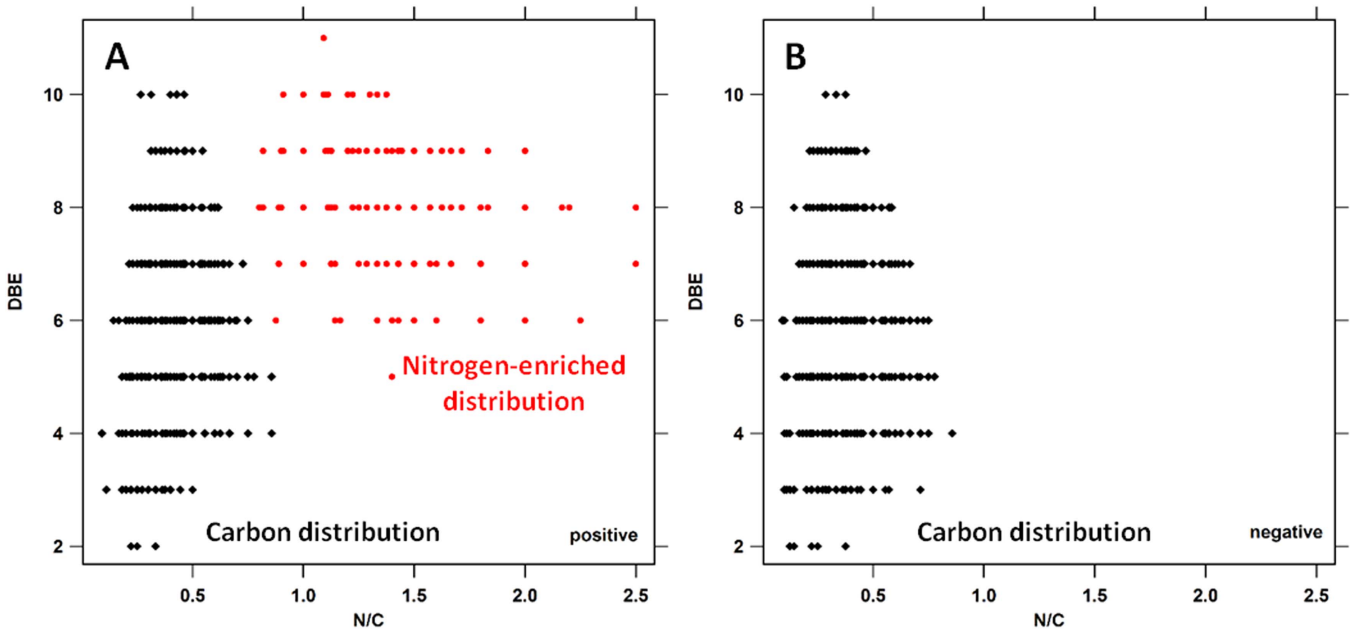

Figure 5. All attributions found in a 3:1:1 (48 hr) residue plotted in DBE vs. N/C ratio diagrams, in the positive (A) and negative (B) ionization modes. Black attributions correspond to the carbon distribution detected in the positive and negative modes. Red attributions correspond to the nitrogen-enriched distribution detected in the positive mode only.

Appendix

VHRMS Data Treatment

The data first need to be cleaned of contamination and data-processing artifacts so that each remaining peak is indeed an ion present in the residue. To do so, we use an in-house software described in Danger et al. (2013, 2016). For each remaining peak, a molecular formula is generated considering all combinations of $C_xH_yN_zO_w$ that follow three restrictions: no adducts except proton adducts are considered, no radical ions are considered, and the valence of elements strictly constrains the solutions. The formula with the nearest m/z value is retained if the corresponding residual is below 1 ppm. Otherwise, the peak is left unassigned. As we use an ESI source that limits fragmentation and provides a smooth ionization, we assume that the calculated formulas correspond to $[M+H]^+$ and $[M-H]^-$ in the positive and negative modes, respectively. We thus subtract one H^+ from the formula in the positive mode and add one H^+ in the negative mode to obtain the formulas of the original molecules. As displayed in the VHRMS analyses section (section 2.2), two distributions are observed after VHRMS data treatment. The attributions of the distribution detected in both modes (the carbon distribution) are averaged together to give the final values. If an attribution is found in both modes, it is only counted once in the average, to avoid giving twice as much weight to molecules that can be ionized in both modes. The attributions of the distribution seen only in the positive ionization mode (the nitrogen-enriched distribution) are averaged together separately. Furthermore, all attributions common with the blank are removed. Once a molecular formula has been assigned to each peak with a residual below 1 ppm, the average values of the DBE and the N/C and O/C ratios of each sample are calculated with the following formulas:

$$\mathrm{DBE} = \frac{\sum_i (2n_{\mathrm{C}_i} + 2 - n_{\mathrm{H}_i} + n_{\mathrm{N}_i})}{\sum_i 2},$$

$$\frac{\mathrm{N}}{\mathrm{C}} = \frac{\sum_i n_{\mathrm{N}_i}}{\sum_j n_{\mathrm{C}_j}},$$

$$\frac{\mathrm{O}}{\mathrm{C}} = \frac{\sum_i n_{\mathrm{O}_i}}{\sum_j n_{\mathrm{C}_j}},$$

where n_{X_k} is the number of element X in the molecular formula attributed to the peak number k and DBE is the double bond equivalent or degree of unsaturation. It should be noted that the same weight is given to all formulas regardless of the intensity of the corresponding peaks. We chose not to weight the formulas with intensities because variations in intensity can be due to factors other than the abundance of the ion, such as the ionization efficiency or the pH (Danger et al. 2016). The elementary ratios and DBE are calculated in the positive and negative ionization modes for each sample. Those ratios are then plotted in diagrams of DBE versus N/C and DBE versus O/C to compare the different samples. Samples were made in triplicates in order to evaluate the standard deviation of the elementary ratios. For the H_2O:CH_3OH:NH_3 3:1:5 residues, the data of only two of the triplicates were exploitable. Indeed, the 3:1:5 ices led to a very small amount of residue compared to the other mixtures, and one of them did not produce enough residue for either IR or VHRMS analyses.

References

Altwegg, K., Balsiger, H., Bar-nun, A., et al. 2016, SciA, 2, e1600285
Bergin, E. A., Blake, G., Ciesla, F., Hirschmann, M. M., & Li, J. 2015, PNAS, 112, 8965
Bernstein, D. I., Sandford, S. A., Allamandola, L. J., et al. 1995, ApJ, 454, 327

Bockelée-Morvan, D., Crovisier, J., Mumma, M. J., & Weaver, H. A. 2004, in Comets II, ed. M. C. Festou, H. U. Keller, & H. A. Weaver (Tucson, AZ: Univ. Arizona Press), 391
Bonnet, J. Y., Thissen, R., Frisari, M., et al. 2013, IJMSp, 354–355, 193
Boogert, A. C. A., Gerakines, P. A., & Whittet, D. C. B. 2015, ARA&A, 53, 541
Bossa, J. B., Duvernay, F., Borget, F., Chiavassa, T., & Theulé, P. 2008, A&A, 492, 719
Briggs, R., Ertem, G., Ferris, J. P., et al. 1992, OLEB, 22, 287
Burton, A. S., Glavin, D. P., Elsila, J. E., et al. 2014, M&PS, 49, 2074
Butscher, T., Duvernay, F., Danger, G., & Chiavassa, T. 2016, A&A, 60, 1
Callahan, M. P., Martin, M. G., Burton, A. S., Glavin, D. P., & Dworkin, J. P. 2014, J. Chromatogr. A., 1332, 30
Cooper, G., Kimmich, N., Belisle, W., et al. 2001, Natur, 414, 879
Cooper, G., & Rios, A. C. 2016, PNAS, 113, E3322
Cronin, J. R., & Moore, C. B. 1971, Sci, 172, 1327
Danger, G., Fresneau, A., Abou Mrad, N., et al. 2016, GeCoA, 189, 184
Danger, G., Orthous-Daunay, F., de Marcellus, P., et al. 2013, GeCoA, 118, 184
de Marcellus, P., Fresneau, A., Brunetto, R., et al. 2017, MNRAS, 464, 114
de Marcellus, P., Meinert, C., Myrgorodska, I., et al. 2015, PNAS, 112, 965
Duvernay, F., Chiavassa, T., Borget, F., & Aycard, J. P. 2005, JPCA, 109, 6008
Elsila, J. E., Glavin, D. P., & Dworkin, J. P. 2009, M&PS, 44, 1323
Fresneau, A., Danger, G., Rimola, A., et al. 2014, MNRAS, 443, 2991
Gautier, T., Schmitz-Afonso, I., Touboul, D., et al. 2016, Icar, 275, 259
Greenberg, J. M., Li, A., Mendozagomez, C. X., et al. 1995, ApJL, 455, L177
Hayes, J. 1967, GeCoA, 31, 1395
Henderson, B. L., & Gudipati, M. S. 2015, ApJ, 800, 66
Le Guillou, C., Bernard, S., Brearley, A. J., & Remusat, L. 2014, GeCoA, 131, 368
Le Guillou, C., & Brearley, A. 2014, GeCoA, 131, 344
Lundell, J., & Räsänen, M. 1997, JMoSt, 436–437, 349
Maçôas, E. M. S., Khriachtchev, L., Fausto, R., & Räsänen, M. 2004, JPCA, 108, 3380
Martins, Z., Modica, P., Zanda, B., & d'Hendecourt, L. L. S. 2015, M&PS, 50, 926
Meinert, C., Myrgorodska, I., De Marcellus, P., et al. 2016, Sci, 352, 208
Muñoz Caro, G. M., Dartois, E., Boduch, P., et al. 2014, A&A, 566 A93
Muñoz Caro, G. M., & Schutte, W. A. 2003, A&A, 412, 121
Nuevo, M., Meierhenrich, U. J., D'Hendecourt, L., et al. 2007, AdSpR, 39, 400
Nuevo, M., Milam, S. N., Sandford, S. A., et al. 2011, AdSpR, 48, 1126
Öberg, K. I. 2016, ChRv, 116, 9631
Öberg, K. I., van Dishoeck, E. F., Linnartz, H., & Andersson, S. 2010, ApJ, 718, 832
Pizzarello, S., Wang, H., & Chaban, G. M. 2010, GeCoA, 74, 6206
Pizzarello, S., & Williams, L. B. 2012, ApJ, 749, 161
Pizzarello, S., Williams, L. B., Lehman, J., Holland, G. P., & Yarger, J. L. 2011, PNAS, 108, 4303
Schmitt-Kopplin, P., Gabelica, Z., Gougeon, R. D., et al. 2010, PNAS, 107, 2763
Schutte, W. A., Boogert, A. C. A., Tielens, A. G. G. M., et al. 1999, A&A, 343, 966
Somogyi, Á, Smith, M. a., Vuitton, V., Thissen, R., & Komáromi, I. 2012, IJMSp, 316–318, 157
Somogyi, Á, Thissen, R., Orthous-Daunay, F. R., & Vuitton, V. 2016, Int. J. Mol. Sci., 17, 439
Theule, P., Duvernay, F., Danger, G, et al. 2013, AdSpR, 52, 1567
Vinogradoff, V., Duvernay, F., Danger, G, et al. 2011, A&A, 530, A128
Vinogradoff, V., Rimola, A., Duvernay, F., et al. 2012, PCCP, 14, 12309